Comparison of Core Ar^{17+} and Mo^{32+} Toroidal Rotation in C-Mod Plasmas

J.E. Rice[‡], C. Angioni[♯], N.M. Cao[†] and M.L. Reinke [♮]

[‡]*PSFC MIT, Cambridge, Massachusetts 02139, USA*

[♯]*Max-Planck-Institut für Plasmaphysik, Boltzmannstr. 2, 85748 Garching, Germany*

[†]*CIMS NYU, New York, New York 10012 USA*

[♮]*CFS, Cambridge, Massachusetts 02139, USA*

Abstract

Core (r/a < 0.5) toroidal rotation from argon (Ar^{17+}, 40 AMU) and molybdenum (Mo^{32+}, 96 AMU) ions has been compared in C-Mod tokamak plasmas over a wide range of operating conditions and confinement schemes, including Ohmic L-mode in the linear and saturated regimes, ICRF heated I-mode and H-mode, as well as in discharges with induced locked modes and with external current and rotation drive. In all cases the velocities of the two impurities are identical within about 5%, for a range between -60 and $+80$ km/s. This is in general agreement with the predictions of neo-classical theory.

1. Introduction

Toroidal rotation in tokamak plasmas exhibits a rich phenomenolgy [1]. Impurity toroidal rotation, whether measured passively in the x-ray or ultra-violet wavelength range, or determined actively using neutral beam-induced visible light emission, has traditionally been used as a proxy for main ion rotation [1]. In neo-classical theory, main ion and impurity toroidal rotation differs, and in principle, a correction can be applied [2]. Recently, main ion toroidal rotation has been directly measured using a sophisticated analysis of charge-exchange spectra, and a comparison with carbon impurity rotation is at odds with neo-classical predictions [3, 4, 5]. Charge-exchange spectroscopy is typically employed for measurements of low Z elements like carbon, and rotation studies of heavier elements usually relies upon x-ray spectroscopy. The edge toroidal rotation of boron (B^{5+}, 10.8 AMU) and carbon (C^{6+}, 12 AMU) was found to be identical in DIII-D plasmas [6]. Comparison of carbon and nickel (Ni^{26+}, 58.7 AMU) toroidal rotation velocities has been made in JET plasmas with neutral beam injection, and the magnitudes were found to be equal within the experimental error of 10%, for a range between 45 and 375 km/s [7]. In C-Mod, the toroidal rotation characteristics of Ar^{17+} and Mo^{32+} were also found to be similar in Ohmic [8] and ion cyclotron range of frequencies (ICRF) heated [9] discharges, and a detailed comparison of their velocities will be presented here. The experimental setup will be summarized in the next section, while in section 3 observations of impurity toroidal rotation in a wide variety of operational regimes will be described in detail. A discussion, along with comparison to theory, will be given in section 4.

2. Experimental Setup

The observations described here were from the Alcator C-Mod tokamak, a compact (major radius R = 0.67 m, typical minor radius $a \sim 0.21$ m), high magnetic field ($B_T \leq 8.1$ T) device with molybdenum plasma facing components [10, 11]. C-Mod had the usual diagnostic complement [12], in addition to 4 MW of ICRF power at $\sim$80 MHz, 1.2 MW of lower hybrid current drive (LHCD) power at 4.6 GHz [13] and external coils for preventing/inducing locked modes. Supplementary to the linear and saturated Ohmic confinement (LOC and SOC) regimes [14], the ICRF power allowed access to I-mode [15, 16] and H-mode [11]. For the present study, a large range of plasma parameters was explored in over 400 discharges: plasma current from 0.4 to 1.2 MA, toroidal magnetic field from 3.0 to 7.8 T, electron density from 0.29 to $3.1\times10^{20}/m^3$, central electron temperature from 0.95 to 4.8 keV and core collisionality ν_* between 0.03 and 0.7. All plasmas were in deuterium unless otherwise noted. With the exception of LHCD and occasional ICRF mode conversion flow drive, there was no external momentum input and the rotation is considered instrinsic. Core impurity emission and rotation velocities from argon and molybdenum ions were obtained from a spatially imaging spherical crystal Johann spectrometer system [17, 18]. Doppler tomography was performed and line shapes were taken to be Gaussian. Argon was introduced (typically at the beginning of discharges) through a piezo-electric valve, and a sufficient

level throughout was maintained by recycling. Molybdenum is an intrinsic impurity and the details of the edge source are not well characterized. For the present study, spectra in the x-ray 3720-3750 mÅ range were used, which contains both the Ar^{17+} Ly_α doublet (1s $^1S_{\frac{1}{2}}$ - 2p $^2P_{\frac{3}{2}}$ at 3731.10 mÅ and 1s $^1S_{\frac{1}{2}}$ - 2p $^2P_{\frac{1}{2}}$ at 3736.52 mÅ) [19, 20, 21] and the Mo^{32+} 4D transition ($2p_{\frac{3}{2}}$ - $4d_{\frac{5}{2}}$ at 3739.8 mÅ) [22, 23]. Upper levels for these transitions are mainly populated through electron impact excitation out of the ground states, and for temperatures below 5 keV, these ions exist near the plasma center. Wavelength calibration for the Johann systems was transferred from several von Hamos spectrometers when they were simultaneously employed. The von Hamos spectrometers were calibrated with an x-ray tube which produced potassium Kα emission [19, 8, 24, 9, 25]. Shown in Fig.1 is a typical line integrated x-ray spectrum used in this analysis. The argon and molybdenum lines are well resolved. Note that the line

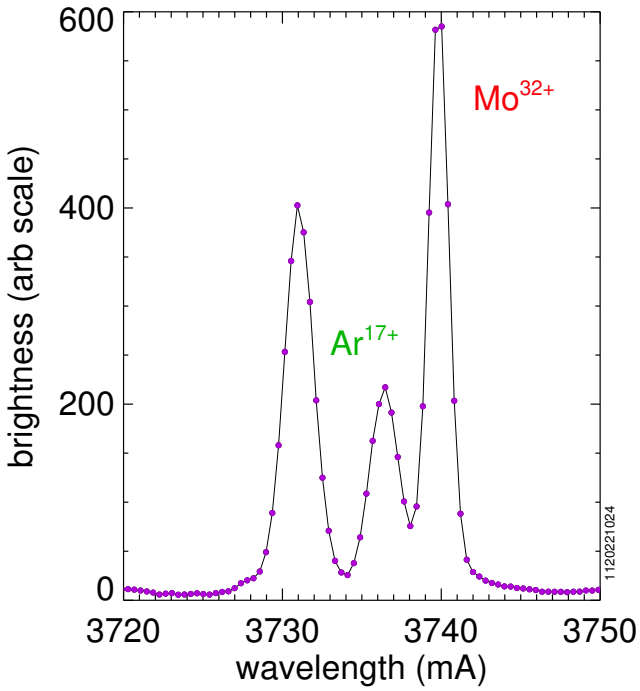

Figure 1: An x-ray spectrum showing the Ar^{17+} Ly_α doublet and the Mo^{32+} 4D transition.

width of the 4D transition is narrower than the Ly_α doublet, due to the higher mass of molybdenum. From the Doppler shifts of such x-ray spectra, the toroidal rotation velocity for both ions can be determined. Shown in Fig.2 are the relevant time histories for a discharge with a locked mode, which brings the core toroidal rotation to a halt. At

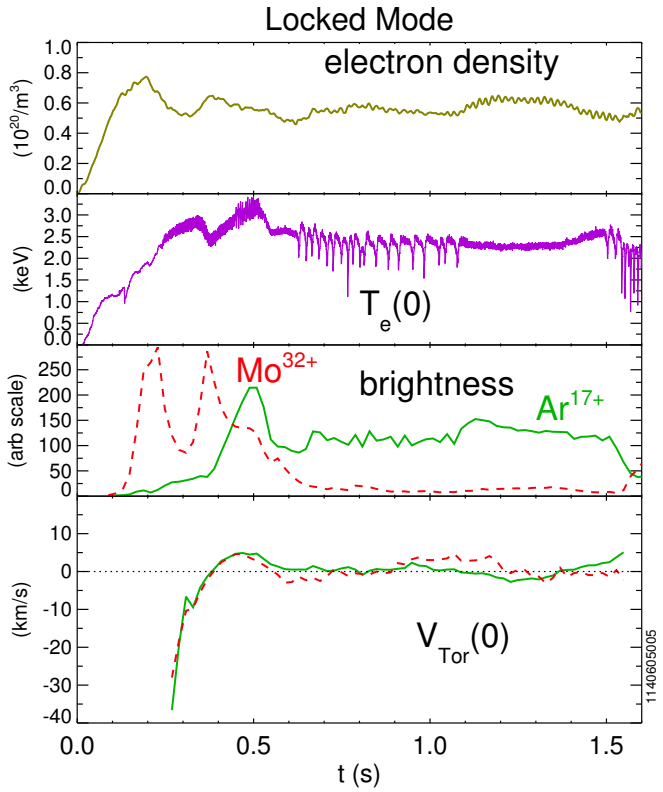

Figure 2: Parameter time histories for a 1.0 MA, 5.4 T discharge with a locked mode (starting at 0.53 s). From top to bottom, the electron density, the central electron temperature, the Ar^{17+} (green) and Mo^{32+} (red dashed) line brightnesses and the central chord line integrated toroidal rotation velocities (bottom frame).

the time of the mode locking (0.53 s), the sawteeth were suppressed and both argon and molybdenum core rotation velocities were near 0. Notice that the Ar^{17+} and Mo^{32+} line brightness time histories are completely different, largely because the edge sources are quite distinct. This holds true for all of the discharges considered here.

3. Impurity Rotation in Different Operational Regimes

In this section, a detailed study of Ar^{17+} and Mo^{32+} rotation, in a variety of operational regimes, will be presented. Shown in Fig.3 are parameter time histories for a discharge in the low collisionality LOC regime. The rotation is typically directed co-

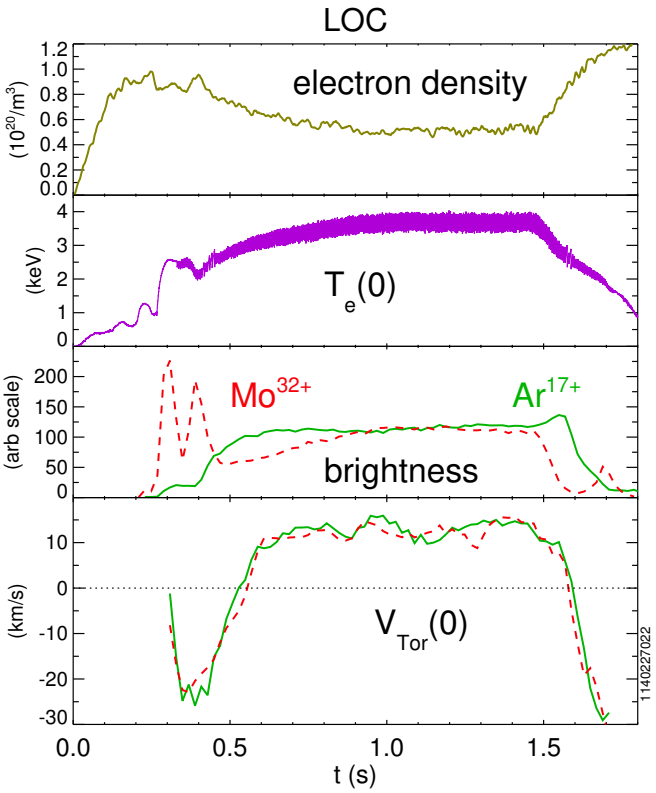

Figure 3: Time histories for a 0.8 MA, 5.4 T discharge in the LOC regime. The legend is the same as in Fig.2.

current with LOC [14], which includes dominance by trapped electron modes (TEMs). In a similar fashion to Fig.2, the argon and molybdenum rotation is nearly identical throughout the discharge. These similarities obtain in the higher density SOC regime, as can be seen in Fig.4. With SOC, the rotation is typically in the counter-current direction [14], where ion temperature gradient (ITG) modes are dominant. As in Fig.3, the

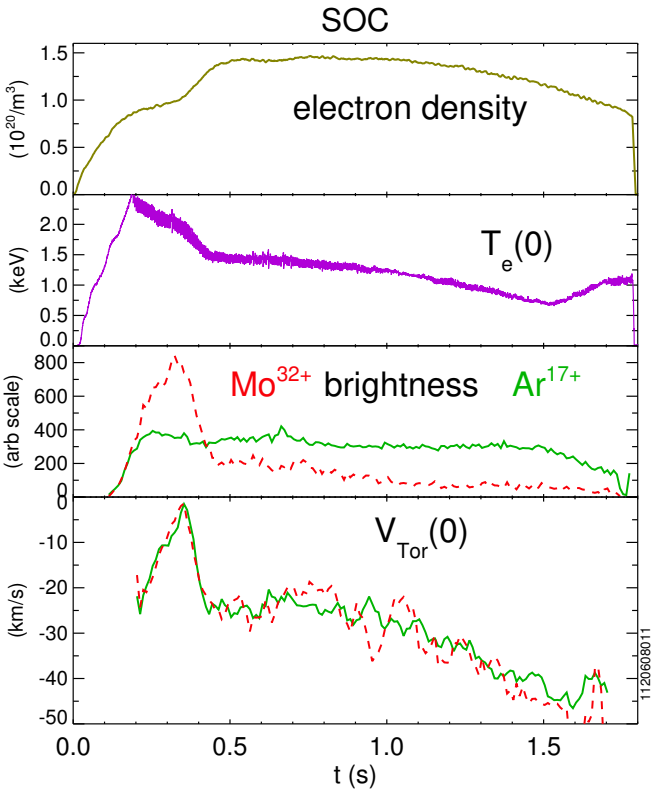

Figure 4: Time histories for a 0.6 MA, 5.4 T discharge in the SOC regime. The legend is the same as in Fig.2.

argon and molybdenum rotation velocities are well matched throughout. The results of Figs.3 and 4 indicate that despite dominance by different types of turbulence, there is no effect on impurity toroidal rotation. The LOC and SOC regimes can be accessed in a single discharge through, for example, a density ramp, which gives rise to a dynamic rotation reversal [14]. An example of this is shown in Fig.5 with a downward density ramp causing a rotation reversal from counter- to co-current at around 0.8 s, when the critical density is reached. Similar to what was seen in Figs.3 and 4, the argon and

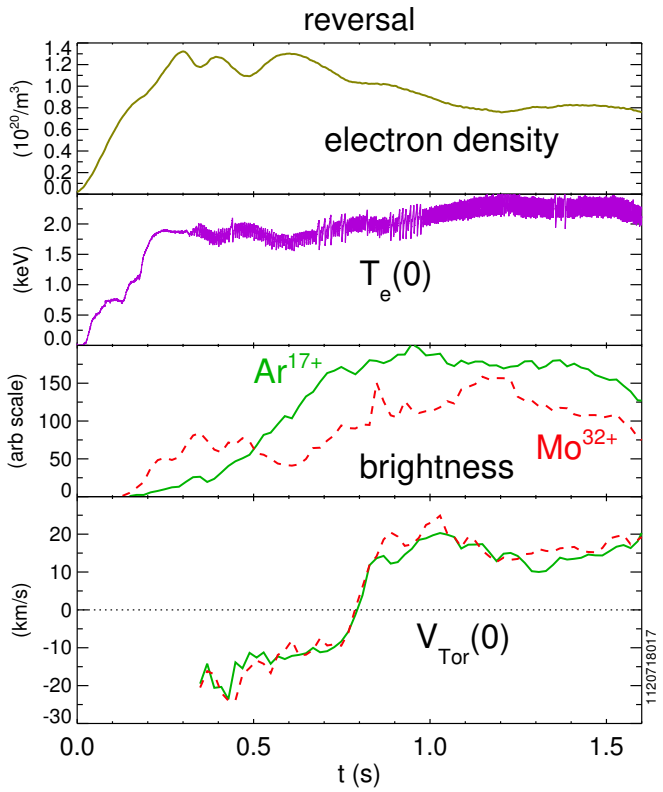

Figure 5: A dynamic rotation reversal from the counter- to co-current direction induced by a downward density ramp in a 1.0 MA, 5.4 T discharge. The legend is the same as in Fig.2.

molybdenum rotation time histories are nearly the same.

Figs.2-5 presented impurity toroidal rotation results in various Ohmic operational scenarios, and there was no strong mass or charge dependence observed in the two regimes dominated by different turbulent modes. It is well known that in enhanced confinement scenarios, the intrinsic rotation is directed co-current [24, 9, 26, 27, 28, 29, 1], driven by the pedestal temperature gradient [28, 29]. Shown in Fig.6 are the parameter time histories of a 1.1 MA, 5.6 T I-mode discharge [15, 28, 11, 16], accessed with 3 MW of ICRF power in the unfavorable magnetic configuration. The argon

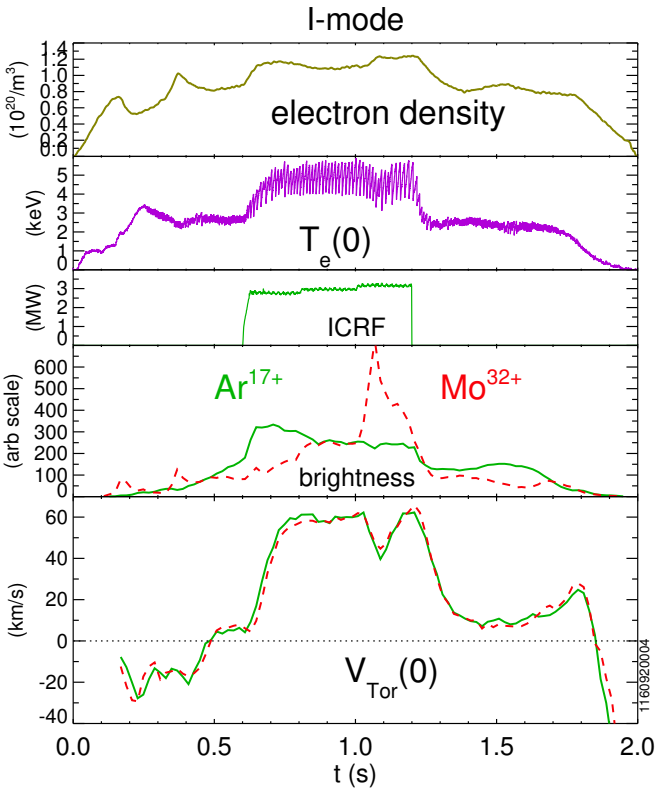

Figure 6: Time histories of a 1.1 MA, 5.6 T I-mode discharge. From top to bottom, the electron density, the central electron temperature, the ICRF power, the Ar^{17+} (green) and Mo^{32+} (red dashed) line brightnesses and the central toroidal rotation velocities (bottom frame).

and molybdenum velocities are nearly identical before, across, during and after the L- to I-mode transition. This includes peculiarities like the drop in rotation after 1.05 s that was due to a molybdenum injection which caused a temporary decrease in the electron temperature. Argon and molybdenum rotation has also been compared in a handful of H-mode discharges, limited in number because H-mode is usually only accessed following a boronization to reduce significantly the molybdenum content of the plasma, and thus there typically isn't enough signal to measure the Mo^{32+} velocity. A rare example for a 0.9 MA 5.5 T discharge is shown in Fig.7, that had two transient ELM-free H-mode periods. In this H-mode case, the argon and molybdenum rotation

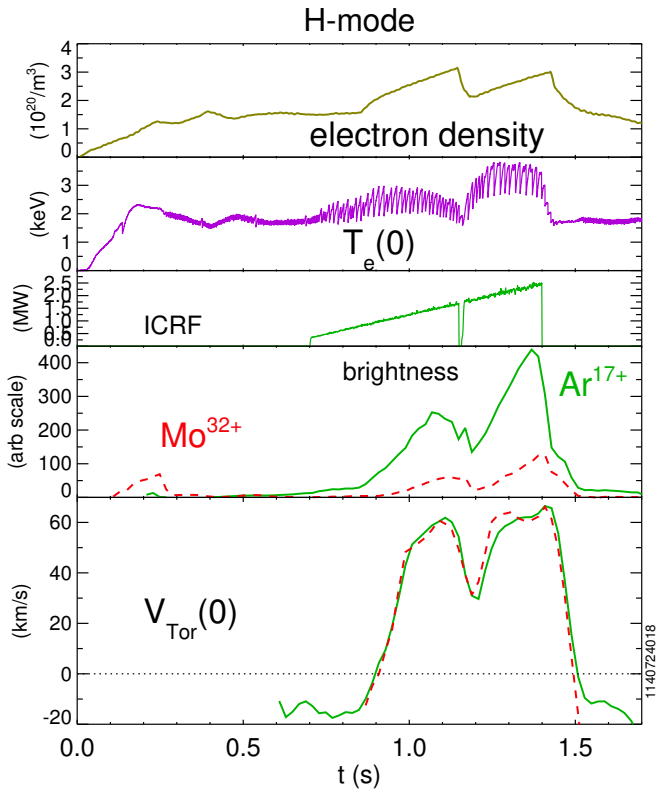

Figure 7: Parameter time histories for a 0.9 MA, 5.5 T H-mode discharge. The legend is the same as in Fig.6.

waveforms are very similar, as was seen in I-mode.

The previous cases of Figs.3-7 featured intrinsic rotation with no external momentum input. Core argon and molybdenum rotation has also been compared in cases with momentum input from RF power injection. LH waves are known to generate counter-current rotation at power levels not high enough for significant current drive, and to feature co-current rotation if the central q value is greater than unity [30, 31]. An example of impurity rotation with LHCD, for a 0.8 MA, 5.4 T discharge is shown in

Fig.8. Following initiation of the LH power, the impurity ions began rotating in the

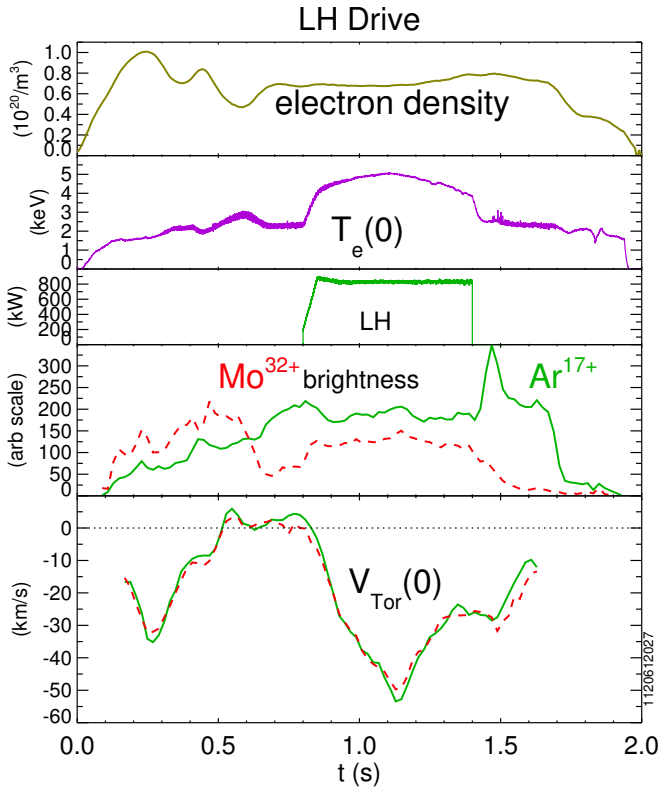

Figure 8: Parameter time histories for a 0.8 MA, 5.4 T discharge with 800 kW of LH power. From top to bottom, the electron density, the central electron temperature, the LHCD power, the Ar^{17+} (green) and Mo^{32+} (red dashed) line brightnesses and the central toroidal rotation velocities (bottom frame).

counter-current direction, the same as the direct momentum input from the waves. Just after 1.1 s, the rotation trended to the co-current direction, as there was a significant change in the current density profile, along with a suppression of sawteeth. Throughout this discharge, the argon and molybdenum velocities tracked very closely. Before the sawtooth suppression $\sim$1.1 s, the q profile was monotonic, with central values below unity, and with weak magnetic shear in the core. After this time, the central safety factor was above 1. Even with these changes in the q profile, the argon and molybdenum rotation remained the same.

ICRF mode conversion flow drive (MCFD) has been shown to generate toroidal rotation [32, 33, 34], and an example for a 1.0 MA, 7.2 T discharge is shown in Fig.9. Similar strong rotation drive is seen in both argon and molybdenum for the highest power level. Unlike the ICRF heated I- and H-mode plasmas, whose intrinsic rotation is generated by a steep pedestal temperature gradient [28], MCFD is due to direct

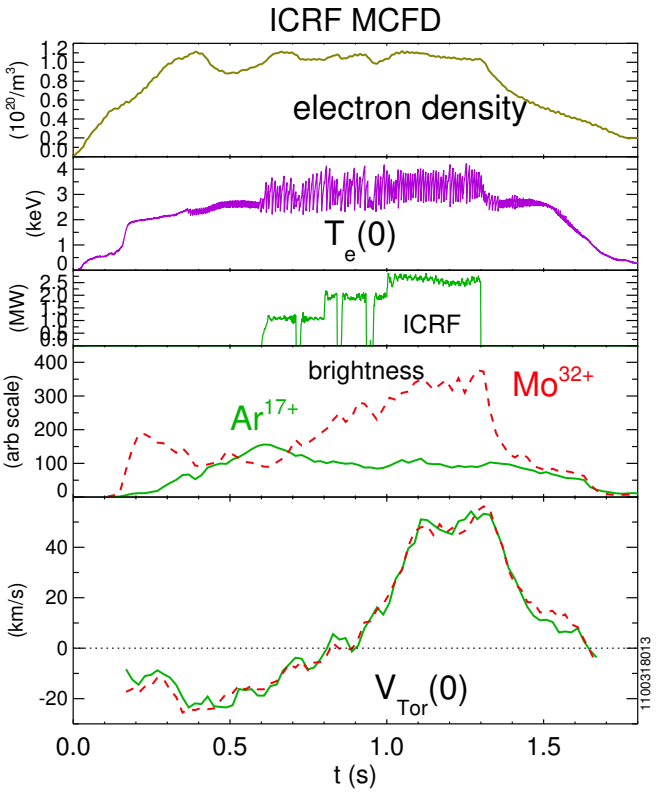

Figure 9: The parameter time histories of a 1.0 MA, 7.2 T discharge with ICRF MCFD. Same legend as in Fig.7.

momentum input from the waves.

A wide body of observations is summarized in Fig.10 which shows the Mo^{32+} rotation as a function of the Ar^{17+} velocity from over 1000 time slices from numerous representative discharges, including the cases shown in Figs.2-9. The molybdenum and

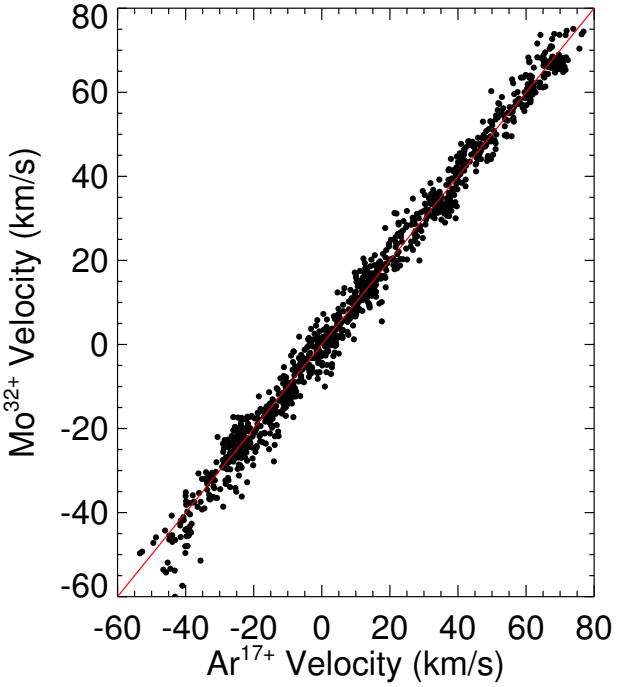

Figure 10: The Mo^{32+} velocity as a function of the Ar^{17+} velocity for over 1000 time slices from a large variety of discharge conditions.

argon rotation velocities match over a range from -60 to $+80$ km/s and a vast majority of the points is within 5%.

4. Discussion and Summary

As has been seen in the previous section, the intrinsic and RF driven impurity toroidal rotation seems to be independent of charge (nearly a factor of two) or mass (more than a factor of two) across a very large operational range (however, the charge to mass ratios of the two impurities, $17^+/40 = 0.43$ and $32^+/96 = 0.33$, only differ by 30%). As a starting point, it would be informative to compare this observation to the predictions of neo-classical theory. For the special case of the impurity toroidal rota-

tion at the magnetic axis in an Ohmic plasma [2] (neglecting the term related to the Spitzer conductivity)

$$V_{\|}^{I} = -\tau_{ii} Z_i e E_{\|} f / m_i \tag{1}$$

where τ_{ii} is the ion-ion Coulomb collision time, $E_{\|}$ is the parallel electric field, Z_i and m_i are the charge and mass of the background ion and f is given by

$$f = \frac{Z_I - Z_i}{Z_I} \frac{\sqrt{2} + 13\alpha/4}{(1+\alpha)(\sqrt{2}+\alpha)} \frac{n_i m_i}{n_i m_i + n_I m_I} \tag{2}$$

where Z_I and m_I are the impurity charge and mass, n_i and n_I are the background ion and impurity densities and α is the impurity strength parameter $\alpha \equiv (n_I\ Z_I^2)/(n_i\ Z_i^2)$. Shown in Fig.11 is the factor f as a function of impurity concentration n_I/n_i for Ar^{17+} and Mo^{32+} in deuterium plasmas. The parameter f is close to unity for reasonable

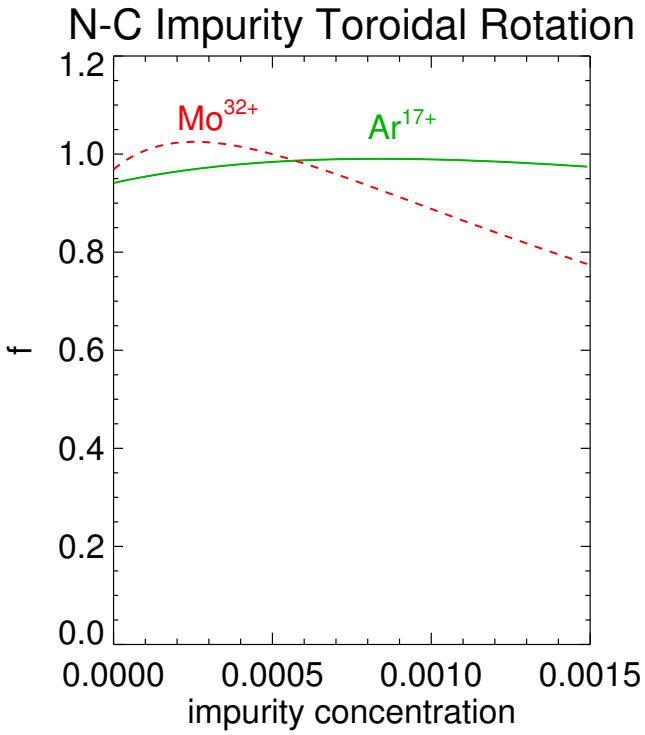

Figure 11: The neo-classical parameter f as a function of impurity concentration n_I/n_i for Ar^{17+} (solid green) and Mo^{32+} (red dashed) in deuterium plasmas.

values of n_I/n_i. A typical impurity concentration for molybdenum in C-Mod plasmas

was $\sim 5\times10^{-4}$ [23], whereas for argon it was $\sim 1.5\times10^{-3}$, depending largely upon the size of the gas puff. The main takeaway if that $f \sim 1$ for both argon and molybdenum, and this is consistent with their observed velocities being equal within 5% as shown in Fig.10.

More generally, the difference between the impurity and main ion rotation frequency is given by Eq.40 of [2] (assuming trace concentrations, in the impurity banana-plateau regime), which is independent of the radial electric field, and depends upon the ion temperature profile and the coefficient K_2, which is a function of the parallel viscosities, including the impurity mass, charge and concentration. By extension, the difference between the argon and molybdenum rotation frequencies is given by

$$\omega_{Ar} - \omega_{Mo} = 3/4(v_{T_i}/R)(\rho_{ip}/L_{T_i})(K_2^{Ar} - K_2^{Mo}) \tag{3}$$

where v_{T_i} is the ion thermal velocity and $\rho_{ip} \equiv m_i c v_{T_i}/Z_i e B_\theta$, with L_{T_i} the ion temperature gradient scale length. K_2 for Ar^{17+} and Mo^{32+} as a function of inverse aspect ratio is shown in Fig.12, where the nominal values of n_I/n_i were taken to be 1.5×10^{-3} and 5×10^{-4}, respectively. As can be seen, there is very little difference between the K_2 values for argon and molybdenum, and as such, very little difference is expected in their toroidal rotation velocities. In the conclusions section of [2], it is stated "Different impurity species rotate with approximately the same speed". Again, this is consistent with the results shown in Fig.10.

The charge and mass dependence of the turbulence driven intrinsic impurity toroidal rotation is unclear for various turbulent regimes. Consistency with this general neo-classical theory expectation suggests that any turbulence drive, which could produce mass or charge dependent differential toroidal rotation of the impurities, has negligible impact. In the plasma core, various turbulent mechanisms [35] can generate a residual stress, which produces an intrinsic rotation of the bulk plasma. Present experimental results suggest that different impurity species follow the bulk plasma rotation, with negligible differences in individual impurity rotation, consistent with the predictions of neo-classical theory. As a companion result, it can be expected that in the core of these plasmas, the poloidal rotation does not differ from the neo-classical expectations significantly, otherwise non-negligible differences would be observed also in the toroidal rotation of the impurities.

5. Acknowledgements

The authors thank J. Irby, J. Hughes and A. Hubbard for electron density and temperature measurements, E. Marmar for providing $Z_{\rm eff}$, T. Stoltzfus-Dueck for enlightening discussions, the ICRF group and the entire C-Mod team for expert operation of the device. Work supported at MIT by DoE Award DE-SC0014264.

References

[1] Rice J.E., 2022 "Driven rotation, self-generated flow, and momentum transport in tokamak plasmas", Springer Series on Atomic, Optical, and Plasmas Physics

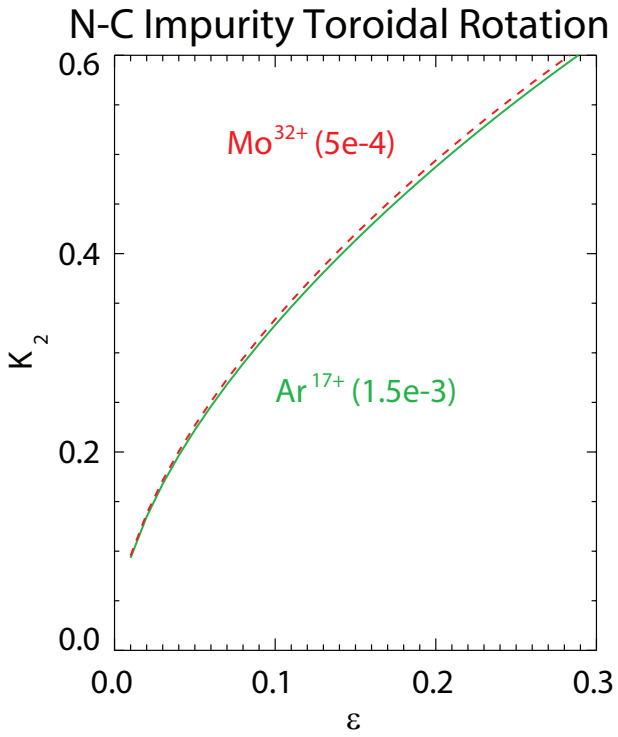

Figure 12: The neo-classical coefficient K_2 as a function of inverse aspect ratio ε for Ar^{17+} (solid green) and Mo^{32+} (red dashed) in deuterium plasmas. The impurity concentration n_I/n_i was taken to be 1.5×10^{-3} for argon and 5×10^{-4} for molybdenum.

119, ISBN 978-3-030-92265-8.

[2] Kim Y.B. *et al.*, 1991 *Phys. Fluids B* **3** 2050.

[3] Grierson B.A. *et al.*, 2012 *Phys. Plasmas* **19** 056107.

[4] Grierson B.A. *et al.*, 2013 *Nucl. Fusion* **53** 063010.

[5] Grierson B.A. *et al.*, 2019 *Phys. Plasmas* **26** 042304.

[6] Kim J. *et al.*, 1994 *Phys. Rev. Lett.* **72** 2199.

[7] Eriksson L.-G. *et al.*, 1997 *Plasma Phys. Control. Fusion* **39** 27.

[8] Rice J.E. *et al.*, 1997 *Nucl. Fusion* **37** 421.

[9] Rice J.E. *et al.*, 1999 *Nucl. Fusion* **39** 1175.

[10] Marmar E.S. *et al.*, 2007 *Fusion Sci. Technol.* **51** 261.

[11] Greenwald M. *et al.*, 2014 *Phys. Plasmas* **21** 110501.

[12] Basse N.P. *et al.*, 2007 *Fusion Sci. Technol.* **51** 476.

[13] Bonoli P.T. *et al.*, 2007 *Fusion Sci. Technol.* **51** 401.

[14] Rice J.E. *et al.*, 2020 *Nucl. Fusion* **60** 105001.

[15] Whyte D.G. *et al.*, 2010 *Nucl. Fusion* **50** 105005.

[16] Hubbard A.E. *et al.*, 2016 *Nucl. Fusion* **56** 086003.

[17] Ince-Cushman A. *et al.*, 2008 *Rev. Sci. Instrum.* **79** 10E302.

[18] Reinke M.L. *et al.*, 2012 *Rev. Sci. Instrum.* **83** 113504.

[19] Marmar E.S. *et al.*, 1986 *Phys. Rev. A* **33** 774.

[20] Rice J.E. *et al.*, 2011 *J. Phys. B* **44** 165702.

[21] Rice J.E. *et al.*, 2018 *Nucl. Fusion* **58** 126008.

[22] Rice J.E. *et al.*, 1995 *Phys. Rev. A* **51** 3551.

[23] Rice J.E. *et al.*, 1996 *J. Phys. B* **29** 2191.

[24] Rice J.E. *et al.*, 1998 *Nucl. Fusion* **38** 75.

[25] Rice J.E. *et al.*, 2004 *Nucl. Fusion* **44** 379.

[26] Rice J.E. *et al.*, 2000 *Phys. Plasmas* **7** 1825.

[27] Rice J.E. *et al.*, 2007 *Nucl. Fusion* **47** 1618.

[28] Rice J.E. *et al.*, 2011 *Phys. Rev. Lett.* **106** 215001.

[29] Rice J.E. *et al.*, 2017 *Nucl. Fusion* **57** 116004.

[30] Rice J.E. *et al.*, 2013 *Nucl. Fusion* **53** 093015.

[31] Rice J.E. *et al.*, 2016 *Nucl. Fusion* **56** 036015.

[32] Lin Y. *et al.*, 2008 *Phys. Rev. Lett.* **101** 235002.

[33] Lin Y. *et al.*, 2009 *Phys. Plasmas* **16** 056102.

[34] Lin Y. *et al.*, 2011 *Nucl. Fusion* **51** 063002.

[35] Stoltzfus-Dueck T., 2019 *Plasma Phys. Control. Fusion* **61** 124003.